A coupled ice-ocean modelling study of the northwest Atlantic Ocean

Sheng Zhang, Jinyu Sheng and Richard J. Greatbatch
Department of Oceanography, Dalhousie University, Halifax, NS, Canada, B3H 4J1

Short title: A COUPLED ICE-OCEAN MODELLING STUDY

RESUBMITTED TO JOURNAL OF GEOPHYSICAL RESEARCH

Abstract.

A coupled ice-ocean modelling system is developed for the northwest Atlantic Ocean based on the second version of the Los Alamos sea ice model and a regional ocean circulation model. The coupled ice-ocean system differs from other coupled systems for the same region mainly in two ways. First, the semi-prognostic method suggested by Sheng et al. (2001) is used in the ocean component. This method adjusts the momentum equation of the ocean component to reduce drift of the modelled ocean state, allowing us to carry out a multi-year simulation. Second, the sea ice component uses the elastic-viscous-plastic ice rheology developed by Hunke and Dukowicz (1997) and Winton's (2000) 3-layer thermodynamics. The coupled system is forced by climatological monthly mean atmospheric forcing at the atmosphere/ocean, atmosphere/ice interface and oceanic forcing at the model open boundaries. The system is integrated for three years. Model results from the third year compare favorably with the observations in the region. The coupled system reproduces reasonably well the phase and magnitude of the annual cycle of sea ice. We demonstrate the effect of the ice heat capacity, previously unaccounted for in earlier model results of this region, in delaying the springtime sea-ice melt on the Labrador and Newfoundland Shelves.

1. Introduction

The northwest Atlantic Ocean (hereinafter NWA) referred to in this study covers the region between -76°E and -30°E and between 35°N and 66°N (Figure 1). It comprises the shallow water of the eastern Canadian shelf from Davis Strait to the Gulf of Maine and the deep water of the Labrador Sea, Labrador and Newfoundland Basins. The Labrador Sea is a semi-enclosed sea, which connects to Baffin Bay in the north through Davis Strait and is bounded by Greenland to the east and by the Labrador Shelf to the west. The Labrador Shelf extends from Hudson Strait to the Strait of Belle Isle. From there the Newfoundland Shelf extends southward to include the broad Grand Banks and the offshore Flemish Cap. Sea ice advances and retreats annually over the Labrador and Newfoundland Shelves. In winter, ice in the NWA reaches the lowest latitude found anywhere in the world (Figure 2). The southward extension of ice in the region is determined mainly by a balance between ice advection from the north, atmospheric forcing and oceanic heat transport. Hence, the ice simulation in the NWA presents an interesting while challenging task, with potential global scale implications, in addition to local navigation and weather effects.

Ikeda et al. (1988) were the first to develop a coupled ice-ocean modelling system for the NWA based on Hibler's (1979) ice model and a mixed layer ocean model with a uniform depth of 30 m. Their ice model consisted of two-categories (ice and open-water), zero-layer thermodynamics (Semtner, 1976) and viscous-plastic ice dynamics. Ikeda et al. (1988) embedded some cold and fresh water on the shelf in the initial ocean state with a specified uniform heat flux of 35 W m^{-2} at the bottom of the mixed layer during the ice formation period. They performed a series of simulations for winter months (December to May), with the same initial ocean conditions but different atmospheric forcing corresponding for each winter. They found that the interannual variability of the simulated ice cover is highly correlated with the atmospheric forcing. They also confirmed the early findings (Symonds, 1986) that sea ice south of 55°N is mainly transported from the north. Nevertheless, all of their experiments were limited to the winter months without multi-year integrations.

With the same ice model, more ocean physical processes were added subsequently to the above coupled ice-ocean modelling system. The additional physics included

limited cross-shelf geostrophic dynamics (Ikeda, 1991), and a more realistic upper-ocean mixed layer and oceanic lateral advection (Yao and Ikeda, 1990; Tang et al. 1999). A three-dimensional Bryan-Cox ocean model (Cox, 1984) was then coupled to the ice model (Ikeda et al., 1996), and the ice categories were later increased from two to ten (Yao and Prinsenberg, 1999). The multi-category ice model was also coupled to a (1/6)° σ-coordinate Princeton Ocean Model by Yao et al. (2000). They found that the simulated ice concentration in the NWA was much improved using a multi-category ice model with more realistic initial ocean conditions. Taking a different direction and for the northern Labrador Sea only, Mysak et al. (1991) used a thermal equilibrium ice sheet model coupled to a reduced gravity ocean model. They found that the offshore ice edge position in the northern Labrador Sea is determined mainly by a balance between the atmospheric cooling and onshore heat flux associated with the wind-driven Sverdrup flow.

We use a different coupled ice-ocean modelling system in this study. The ocean component of our coupled system uses the semi-prognostic method introduced by Sheng et al. (2001) to reduce the ocean model drift in multi-year simulations. The sea ice component is the second version of the Los Alamos Sea Ice Model (CICE, Hunke and Lipscomb, 2000), which employs Hunke and Dukowicz's (1997) elastic-viscous-plastic ice rheology and Winton's (2000) three-layer thermodynamics. We show in this paper that the inclusion of the heat capacity of sea ice alters the phase and magnitude of the seasonal ice cycle and reduces the early and excessive ice melting in spring in the NWA, which is a common problem shared by all the previous studies for the same region.

Our focus in this study is mainly on the thermodynamical processes of the coupled system, instead of trying to get a best fit of model results to the observations. The plan of this paper is as follows. Section 2 presents the coupled ice-ocean modelling system. Section 3 discusses the effects of the ice heat capacity on the phase and magnitude of the springtime sea ice melting, and also examines the sensitivity of model results to the sea surface temperature and the net heat flux at the air-sea interface over the areas where ice is present (hereafter the "ice-presence" areas). A summary and discussion of results are presented in section 4.

2. The coupled ice-ocean modelling system

2.1 The regional circulation model of the Northwest Atlantic Ocean

The ocean component of the coupled ice-ocean modelling system used in this study is the regional ocean circulation model of the NWA developed by Sheng et al. (2001). This regional ocean circulation model is based on the three-dimensional primitive-equation z-level model known as CANDIE (Canadian version of DieCAST, Sheng et al., 1998). CANDIE has successfully been applied to various modelling problems on the shelf, including wind-driven circulation over an idealized coastal canyon (Sheng et al., 1998), nonlinear dynamics of a density-driven coastal current (Sheng, 2001), tidal circulation in the Gulf of St. Lawrence (Lu et al., 2001) and wind-driven circulation over a stratified coastal embayment (Davidson et al., 2001). Most recently CANDIE has been applied to the western Caribbean Sea by Sheng and Tang (2003). The reader is referred to Sheng et al. (2001) for discussion of the governing equations and sub-gridscale mixing parameterizations used in the NWA application of CANDIE.

The model domain covers the NWA (Figure 1), with a horizontal resolution of $(1/3)^\circ$ in longitude by $(1/3)^\circ \cos\phi$ in latitude (ϕ) and 31 unevenly spaced z-levels in the vertical. At the model solid boundaries, the normal flow, tangential stress of the currents and horizontal fluxes of temperature and salinity are set to zero. Along the model open boundaries, the normal flow, temperature and salinity fields are calculated using the adaptive open boundary conditions. First, an explicit Orlanski (1976) radiation condition is used to determine whether the open boundary is passive (information leaving the domain) or active (information entering the domain). If the open boundary is passive, the model prognostic variables are radiated outward. If the open boundary is active, the model prognostic variables at the open boundary are restored to the monthly mean climatologies at each z-level with a time scale of 30 days. Furthermore, the depth-mean normal flow across the model open boundaries is set to be the same as in the diagnostic calculation for the North Atlantic of Greatbatch et al. (1991), apart from an additional 2 cm s^{-1} inflow that is specified over the shelf at the Denmark Strait transect (see Figure 1).

The regional ocean circulation model uses the semi-prognostic method to reduce drift of the modelled ocean state in a multi-year simulation. This method adjusts the momentum equation by replacing the model density variable ρ in the hydrostatic equation by a linear combination of the model-computed density ρ_m and an input density ρ_c (Sheng et al., 2001; Greatbatch et al., 2004):

$$\frac{\partial p}{\partial z} = -g\left[\alpha\rho_m + (1-\alpha)\rho_c\right] \equiv -g\rho_m - g(1-\alpha)(\rho_c - \rho_m), \tag{1}$$

where $\rho_m = \rho(T, S, p_{ref})$ is the density calculated from the model potential temperature T and salinity S, and p_{ref} is vertically dependent reference pressure, α is the linear combination coefficient set to 0.5 in this study, and the input density ρ_c is computed from a climatology of hydrographic data. The term $-g(1-\alpha)(\rho_c - \rho_m)$ in (1) is the correction term used to correct for model systematic error and unresolved processes in a multi-year simulation. As stated in Sheng et al. (2001), the above procedure is equivalent to adding a forcing term to the horizontal momentum equation of the ocean model.

There are two major modifications made to the original configuration of the NWA ocean circulation model developed by Sheng et al. (2001). First, the monthly mean climatology of the freshwater flux (difference between evaporation and precipitation) constructed by da Silva et al. (1994) is used to force the ocean model, in addition to the sea surface salinity restoring term already implemented. Second, the restoring time scale for the sea surface temperature and salinity is increased from 15 days to 30 days. The 30-day time scale is about the same as that derived from the scale analysis by Haney (1971) under a given specified constant atmosphere. If atmospheric feedback is considered, the time scale should be even longer (Zhang et al., 1993).

2.2 The Los Alamos sea ice model (CICE)

The sea ice component of our coupled system is the second version of the CICE ice model (Hunke and Lipscomb, 2000). A feature of the model is the use of the second-order MPDATA scheme (Multidimensional Positive Definite Advection Transport Algorithm, Smolarkiewicz, 1984) for calculating ice concentration and associated state variables.

The thermodynamic component of CICE is the 3-layer thermodynamic model

developed by Winton (2000), which is a modified version of Semtner's (1976) 3-layer thermodynamic model. The heat capacity of the upper ice layer in Winton's ice model is defined as a function of temperature to mimic brine pocket effects and that of the lower layer is set to be a constant. The heat capacity of sea ice, which is defined as the energy needed to raise the temperature of a unit mass of sea ice by 1°C, includes not only the energy required to raise the temperature of pure ice but the energy needed to raise the temperature of brine and to melt ice along the walls of brine pockets (Bitz and Lipscomb, 1999). On the top surface of the ice, or snow if any, conductive heat flux though the ice and snow balances the total net incoming heat flux. The latter consists of the sum of specified short and downward long wave radiation, together with sensible and latent heat fluxes and outgoing long wave radiation calculated from the prognostic ice surface temperature. The atmospheric forcing fields (e.g. the surface air temperature - see subsection 2.3) are taken from the half by half degree monthly average data set constructed by da Silva et al. (1994). The model parameterizations to calculate the fluxes over the ice-covered region are the same as in Hunke and Lipscomb (2000).

The heat balance on the top surface of the ice or snow determines the top surface temperature. The exception is when the balanced temperature is above freezing, in which case the top surface temperature is set to the freezing point and the excess part of the heat flux is used to melt snow and ice. On the bottom of the ice, the ice temperature is set to the freezing point of sea water $T_f = -0.055S$, where S is the sea surface salinity. The ice is divided into two equal thickness layers, with a snow layer added on the top of the ice. The high albedo and low conductivity of snow are accounted for but the heat capacity of the snow is neglected. Given the temperature at the previous time step and heat capacity of the ice, the 3-layer thermodynamic ice model solves implicitly for the conductive flux within the ice, temperature at the top surface of the ice/snow and the temperature at the middle of both ice layers. The difference between the conductive flux in the lower ice layer and the ice-ocean interface flux is used to freeze or melt the ice at the ice-ocean interface. The ice-ocean interface flux is proportional to the difference between the temperature of the top ocean layer and the freezing temperature of seawater T_f.

Previous studies show that a single-category thermodynamic ice model produces

little ice volume since the ice concentration is always 100% in a grid cell with ice (e.g. Zhang et al., 1995). In reality, growth and accretion in the open water part of the grid cell (including leads and cracks) contribute significantly to ice growth. To include this lateral growth, a two-category (open water and thick ice) ice model was developed (Thorndike et al., 1975; Hibler, 1979), in which ice growth in the open water category at any time step is immediately converted to thick ice by conserving the ice volume. The ice concentration produced by this two-category ice model is often underestimated due to the conversion, since the new ice is assumed to have a relatively large thickness and hence a small area when it is combined with the thick ice. The simulated ice volume produced by the two-category ice model is likewise overestimated due to the resulting larger portion of open water and thus more heat loss from the ocean (Ikeda et al., 1988). To remedy this, a multi-category ice model was introduced. Some previous studies show that the simulated ice concentration is improved by using a model with five to ten ice categories, in comparison with the two-category ice model (Yao and Prinsenberg, 1999; Yao et al., 2000; Lipscomb, 2001; Bitz et al., 2001). Other studies have found, on the other hand, that the simulated ice conditions using a seven-category ice model are comparable to the results using a two-category ice model (Hibler and Walsh, 1982; Walsh et al., 1985).

The second version of CICE has five ice thickness categories (Lipscomb, 2001) in the standard configuration, with ice growing in open water transferred immediately to the thinest ice. In this study, only two ice categories (thick ice and thin ice/open water) are specified in the CICE ice model in order to resemble closely Hibler's two-category ice model. Different from the conventional two-category ice model discussed above, the thin ice in CICE stays until its thickness grows over a given threshold value (10 cm in this study, same as Hunke and Lipscomb, 2000) and becomes part of the thick ice, or is melted below a given threshold value and thus becomes open water. Due to the nonlinearity of the conductive heat flux, the vertical growth of the ice in CICE is higher than that produced by a single-category ice model due to the presence of thin ice, but lower than that produced by the conventional two-category ice model due to less open water.

The sea ice rheology of CICE is elastic-viscous-plastic, which is numerically more efficient in comparison with the viscous-plastic rheology of Hibler's (1979) model. Since

CICE is solved explicitly with small time steps, the model responds to forcing more quickly and thus is physically more realistic when atmospheric forcing has a short hourly or daily time scale (Hunke and Dukowicz, 1997). All parameters of the ice dynamics take the standard values from Hunke and Lipscomb (2000) and are kept fixed in this study (Table 1). [The effects of ice dynamical parameters have been extensively examined in the past (e.g., Holland et al., 1993; Hunke and Dukowicz, 1997) in polar and high-latitude regions including the NWA (Ikeda et al., 1996; Tang et al., 1999; Yao at al., 2000)].

To account for the effects of the ice generated outside of the model northern boundary, the ice thickness along the northern open boundary of both the Labrador shelf and the east Greenland shelf in the control run is restored to a value of 2 m in winter whenever the thickness produced by the model is less than this value.

The ocean and ice components of the coupled ice-ocean system are kept as independent as possible, with information between the ice and ocean components exchanged once per model day. The variables passed from the ocean model to the ice model are the sea surface temperature, salinity, and the horizontal components of the surface currents. The variables passed from the ice model to the ocean model are ice concentration, heat and freshwater fluxes, and momentum fluxes (i.e., ice stress). These fluxes are used partially or totally, according to the ice concentration, replacing the counterpart fluxes from the da Silva et al. data set (e.g., ice stress to replace wind stress) to force the ocean component for the ice covered portion of the grid points.

2.3 Treatment of the net surface heat flux seen by the ocean

In ice/ocean modelling studies, it is common to calculate the sensible, latent heat fluxes and outgoing long wave radiation (in what we call "the temperature method") based on given, specified sea surface atmospheric variables at 10 m (the most important of which is the surface air temperature), together with specified fluxes such as solar and downward long wave radiations. The temperature method is the most widely used in previous coupled ice/ocean modelling studies (Hibler and Walsh, 1982; Ikeda et al., 1988; Oberhuber, 1993; Hunks and Lipscomb, 2000; Saucier et al., 2003). In the ice-free region, Haney (1971) demonstrated that the net air-sea heat flux can be approximated by a

specified net heat flux plus a restoring term to account for the feedback from the ocean state (we call this as "the flux method"). In this paper, the temperature method is used in our coupled system to calculate the fluxes over ice, as in the original CICE model, but the flux method is used over ice-free areas and the open water portion of grid points containing ice, as described below.

Over ice-free areas, we follow Haney (1971) and linearize the net heat flux through the sea surface ($Q_{\rm net}$) around the climatological sea surface temperature ($\rm SST^{clim}$) to represent the model sea surface temperature ($\rm SST^{model}$) feedback on the sea surface heat fluxes:

$$Q_{\rm net} \approx \hat{Q}_{\rm net} + \beta \left(SST^{\rm clim} - SST^{\rm model} \right) \tag{2}$$

where $\hat{Q}_{\rm net}$ is the net heat flux felt by the ocean without considering the temperature feedback (taken from the da Silva et al. (1994) climatology, as in Sheng et al. (2001)), and β is a coefficient defined as $\Delta z_1 \rho_o c_p / \tau_Q$, where Δz_1 is the thickness of the top z level, c_p is the specific heat, ρ_o is a reference density and τ_Q is the restoring timescale which is set to 30 days as mentioned in subsection 2.1.

In areas where ice is present, we continue to use (2) to parameterize the surface heat flux seen by the ocean, except that now $\hat{Q}_{\rm net}$ is modified to take account of the ice. It should be noted that the restoring term on the RHS of (2) is applied everywhere, including under the ice. The sensitivity of our model results to this term is discussed in subsection 3.3. To parameterize $\hat{Q}_{\rm net}$, we define $Q_{\rm ao}$ as the net heat flux (without temperature feedback) at the air-ocean interface both for the grid points without ice and for the open water portion of the grid points with ice, and $Q_{\rm io}$ as the net heat flux at the ice-ocean interface. Over an ice-free area, $\hat{Q}_{\rm net}$ is the same as $Q_{\rm ao}$. Over an ice-presence area, on the other hand, $\hat{Q}_{\rm net}$ is a linear combination of $Q_{\rm ao}$ and $Q_{\rm io}$. It should be noted that $Q_{\rm ao}$ could differ significantly from $\hat{Q}_{\rm net}$ over the ice-presence area. As an example, we consider an area where the ice concentration is 90%, the net heat flux felt by the ocean ($\hat{Q}_{\rm net}$) is -40 W $\rm m^{-2}$, and the net heat flux at the ice-ocean interface ($Q_{\rm io}$) is -10 W $\rm m^{-2}$. Based on the heat budget, the net heat flux at the air-ocean interface ($Q_{\rm ao}$) over the open-water portion of the ice-presence area is -310 W $\rm m^{-2}$. Therefore, in magnitude, the net air-ocean heat flux over the open water portion is about 8 times larger than the

averaged net heat flux felt by the ocean over the entire grid box and 31 times larger than the heat flux under the ice covered part of the grid box.

The climatological monthly mean net heat flux at the sea surface constructed by da Silva et al. (1994) includes, to a certain degree, the insulation effect of the observed ice. This is expected since their net heat flux climatology was constructed mainly from in situ measurements under a constraint that the global mean heat flux is zero. However, there are more in situ observations over the open water than over the ice-covered areas in the NWA. This is mainly because ships have been major collectors of the measurements and the fair weather bias is well known. Therefore, da Silva et al.'s net heat flux climatology should bias notably toward the measurements in the open water.

To take account of the possible bias of the da Silva et al.'s heat flux, we parameterize $\hat{Q}_{\rm net}$ over the ice-presence area in terms of the climatological sea surface net heat flux constructed by da Silva et al. ($Q_{\rm net}^{\rm clim}$) as

$$\hat{Q}_{\rm net} = (1 - \gamma c) Q_{\rm net}^{\rm clim} + c Q_{\rm io} \tag{3}$$

where c is the ice concentration, and $Q_{\rm io}$ is again the heat flux at the interface between the ice and the ocean, which is proportional to the difference between the freezing temperature and the top ocean model level temperature. The main purpose of introducing γ in (3) is to account for the difference between the da Silva et al. climatological net heat flux and the actual net heat flux at the air-sea interface over the ice-presence areas. The value of γ is set to unity if the da Silva et al. heat flux climatology ($Q_{\rm net}^{\rm clim}$) is constructed from observations made only over the open water portions of the ice-presence areas. A value between 0 and 1 implies that the da Silva et al. climatology includes some influence from the insulation effect of the ice. The value of γ is set to 0.9 in the numerical experiments presented in this paper except where indicated otherwise. In this case, the ice-ocean system sees 100% of the da Silva et al. net heat flux ($Q_{\rm net}^{\rm clim}$) over ice-free areas, and the percentage decreases linearly with increasing model-predicted ice concentration, to 10% in fully ice-covered areas. The sensitivity of the model results to the choice of γ is discussed further in subsection 3.3.

3. Model Results

The coupled ice-ocean system is integrated for three years from a state of rest. The simulated ice and ocean states in the second year are very similar to those in the third year. Model results from the third year are presented in this paper, except where otherwise noted.

3.1 Seasonal evolution of sea ice in the northwest Atlantic

Figure 3 presents the simulated monthly mean ice states in the control run. Sea ice starts to form over the northwestern part of the Labrador Sea in December (Figure 3). Ice coverage expands significantly southward and offshore from January to March, with the offshore ice edge confined roughly at the shelf break. The monthly mean ice thickness produced by the model is about 0.5 m in February and 1 m in March over the Labrador and Newfoundland Shelves. The ice velocity in these three months is southeastward, with a typical speed of 10 cm s^{-1}. The sea ice reaches the northern part of Grand Banks at about 49°N in April and then retreats northward in May and June. Only a very small amount of ice is left over the northwest corner of the Davis Strait in July.

Observations of ice coverage and thickness (Symonds, 1986; Peterson, 1987; Carsey et al., 1989; Prinsenberg et al., 1996) indicate that sea-ice is largely confined to the Labrador and Newfoundland Shelves with a typical ice thickness of about 1 m in winter months. Our simulations are in general agreement with these observations. Also, in comparison with Figure 2, the simulated ice coverage and the position of offshore ice edge (Figure 3) are in good agreement with the climatology. We should point out that the flux method (subsection 2.3) used to drive the ocean model in this study has no direct nudging to ensure the correct ice edge in the model, thus demanding higher model skill to simulate correctly the seasonal cycle of the ice (although there is still a weak, indirect "nudging" through the restoring term added to the heat flux seen by the ocean - see equation (2) and the sensitivity analysis in subsection 3.3). Large differences occur between the observed and simulated ice conditions mainly over two small isolated regions. The coupled system produces almost complete ice coverage in the first winter but is nearly ice free after the first model year in the Gulf of St. Lawrence (GSL). This is mainly because the

simulated sea surface winter temperature in the GSL remains above freezing after the first model year. The reasons for the above-freezing model winter temperatures are not clear, although contributing factors could include the relatively coarse model resolution, less reliable surface heat flux over the GSL in the da Silva et al. climatology, and exclusion of the ice and cold water influxes from the St. Lawrence River. This issue is discussed further in subsection 3.4. The other area where the ice simulation is poor is the East Greenland Shelf. As mentioned in subsection 2.2, the ice thickness along the northern open boundary of both the Labrador Shelf and the East Greenland Shelf in the control run is restored to a value of 2 m in winter whenever the ice produced by the model is less than this value. On the east coast of Greenland, however, the ocean model does not resolve the cool, along-shore East Greenland Current that should flow away from the boundary, carrying the sea-ice with it. The much warmer Irminger Current from the east dominates the area instead (Figure 4), with the result that the ice from the restoring zone near the northern boundary in this region melts within a short distance.

As stated in the introduction, Ikeda et al. (1988) were the first to simulate the interannual variability of the sea-ice cover in the NWA using Hibler's dynamic and thermodynamic ice model. Their ice model consisted of two categories: thick ice and open water, which implies that sea ice formed in the open water category immediately merges to the thick ice category at each time step, thus leaving the open water category to be ice free. The winter mean ice concentration calculated by Ikeda et al. is about 40% on the shelf, which is too low in comparison with the observations made in the region. By contrast, the present coupled ice-ocean system produces lower ice thickness but much higher ice concentration (more than 90% in our model results) in the winter months over the Labrador and northern Newfoundland Shelves.

To illustrate the role of the ice dynamics and thermodynamics, we examine the winter mean net heat flux at the ice-ocean interface (Q_{IO}), which is proportional to the difference between the freezing temperature (T_f) and sea surface temperature. The difference between the ice-ocean net heat flux, Q_{io}, and the conductive flux through the ice provides some of the thermal energy to form or melt ice. The conductive flux is usually small and ignored in the following discussion for simplicity. A positive ice-ocean heat flux indicates

that the sea surface temperature is colder than the freezing point, and therefore that sea ice is forming locally. A negative ice-ocean heat flux, on the other hand, indicates that sea ice over this area is not being generated locally, but rather horizontal transport of sea ice is important. Figure 5a shows that the net heat flux at the ice-ocean interface is positive over Davis Strait and the inner and middle Labrador Shelf, indicating the importance of the local thermodynamics in generating ice over these areas. Over the other ice-presence areas, however, the net heat flux at the ice-ocean interface is near zero or negative, indicating that the sea ice over these areas is mainly transported from other areas.

The winter-mean wind stress used to drive the coupling system (Figure 5b) is roughly southeastward in the Labrador Shelf except the coastal region near 62°N. The ice-ocean stress, on the other hand, is roughly northward (Figure 5a), which is opposite to the directions of both the surface wind stress and ocean circulation (Figure 4) in the region. The fact that the sea-ice is acting as a drag on the ocean means that the sea-ice is being carried southward at least partly by the ocean currents, in addition to the wind stress.

3.2 Heat capacity of the sea ice

Early and excessive ice melting in spring is a common problem in previous modelling studies for the NWA. Ikeda et al. (1988) suggested that this early spring melting problem could be explained partially by the unresolved effect of snow cover and brine pockets, which reflects and absorbs the short wave radiation and hence delays the early spring melting. Ikeda et al. (1996) also speculated that the two-category ice model with low ice concentrations could lead to excessive short wave radiation absorption in the open water, although the problem still existed when the ice albedo was also used in the open water. With high snow albedo and a more realistic initial ocean state, Yao and Prinsenberg (1999) and Yao et al. (2000) demonstrated that a ten-category ice model improved the ice concentration significantly, but the model was still not able to eliminate the problem of early and excessive springtime melting.

Previous modelling studies use Semtner's zero-layer thermodynamic ice model which does not take account of the heat capacity of the sea ice. In the present study, we use Winton's 3-layer thermodynamic model which includes the effect of the heat capacity. The

inclusion of the heat capacity in the model allows the rate of change in ice temperature to be calculated realistically based on the fact that energy is used to raise the ice temperature to the freezing point before the energy is used to melt ice, therefore delaying the melting process. To demonstrate the effect of the ice heat capacity, we generate a zero-layer thermodynamic model from Winton's 3-layer thermodynamic model by ignoring the internal temperature values of the two ice layers and computing the conductive heat flux through the ice using the top and bottom surface temperatures and effective thickness of ice and snow, which is exactly the same as in Semtner's zero-layer model. We couple this zero-layer ice model to the regional ocean circulation model and integrate this zero-layer coupled system for three years. All the other model parameters are same as those in the control run. We compare the zero-layer ice model results with those in the control run. The inclusion of the heat capacity of sea ice affects notably the phase and magnitude of the seasonal cycle of sea ice in the NWA (Figure 6). In comparison with the 3-layer ice model results, the zero-layer ice model results have significantly smaller ice-covered area and smaller ice volume in spring (shaded areas in Figure 6). The springtime ice melting is about 10 days earlier if the heat capacity of sea ice is not included. It should be noted that the same zero-heat-capacity snow layer is used in the 3-layer and zero-layer ice models. It follows that the snow layer is not responsible for the reduction of the early spring sea ice melting shown in Figure 6. Furthermore, since the two model versions differ only in that one takes account of the heat capacity of the ice and the other does not, the reduction in the early spring ice melt can only be a consequence of taking account of the heat capacity in the Winton 3 layer model.

3.3 Sensitivity to the treatment of the net surface heat flux seen by the ocean

The parameterization for $\hat{Q}_{\text{net}}$ in the ice-presence areas was discussed in subsection 2.3. Here we begin by discussing the sensitivity of the model results to the parameter γ in (3). Figure 7 shows the model results for the cases of $\gamma = 0$, 0.5 and 1, corresponding to cases in which 100%, 50% and 0% of the climatological net heat flux constructed by da Silva et al. is allowed to reach the ocean water directly through the ice. The model parameters in these three cases are the same as those in the control run, except that the

ice inflow at the northern open boundary is set to zero. Since the atmospheric heat fluxes in winter are negative in the NWA, the higher the percentage of the net heat flux that reaches the ocean (i.e., smaller γ), the lower the ocean surface temperature and therefore the more sea ice is produced. A comparison of the model results in the three cases (Figure 7) indicates that the coupled system produces thicker ice and therefore greater ice volume for smaller values of γ. The simulated ice coverage and position of the offshore ice edge are less sensitive to the values of γ.

As shown in (2), the net heat flux used to force the ocean model also includes a restoring term $\beta(SST^{\text{clim}} - SST^{\text{model}})$, which is linearly proportional to the difference between the climatological and model calculated SST. This restoring term represents a heat source or sink under sea ice. Even though a weak restoring of 30 days timescale is used in this study, the restoring term has its effects on the simulated ice conditions that deserve some discussion. Two numerical experiments are conducted to examine the sensitivity of the treatment of this restoring term under sea ice. In the first experiment (Figure 8), the γ value is set to unity and ice inflow at the northern open boundary is set to zero. The model SST in this experiment is restored to the value of 1°C colder than the climatological SST wherever ice is present in the climatology shown in Figure 2. In comparison with the control run, in which the model SST restored to the climatological SST, the results demonstrate that the lower the specified temperature used in the restoring term (2), the more sea ice is produced by the coupled system (Figure 8).

In the second experiment, we replace the coefficient β in the restoring term by $(1-\gamma c)\beta$ with $\gamma = 0.9$. Physically, this is equivalent to treating the restoring term as part of the net air-ocean heat flux forcing so that it is subject to the same reduction due to the presence of sea ice. The ice inflow at the northern open boundary in this experiment is also set to zero. Figure 8 shows that there is a much greater amount of sea ice over the Labrador and Newfoundland Shelves produced in this experiment, particularly in later winter and spring, in comparison with that in the control run (Figure 3).

3.4 Flux versus temperature methods

There is a major difference in the amount of information regarding the observed ice distribution contained in the flux and temperature methods described in subsection 2.3. The surface air temperature in winter over the open water in the study region will not be far from the water temperature, i.e., around the freezing point, but is significantly colder over ice. Due to this difference, use of the temperature method provides the model with information on the climatological sea ice distribution. In other words, the observed atmospheric temperature contains information on the location of the observed ice, and it would nudge the model to form ice over areas where sea ice is present in the data (where low atmospheric temperatures are observed). By contrast, the flux method does not contain such direct nudging.

To demonstrate the effect, we reformulate our model forcing to imitate the nudging effect present in the temperature method. Let $Q_{\rm air}$ be the observed heat flux averaged over a grid point seen by the atmosphere and $Q_{\rm con}$ be the conductive heat flux through the ice. We now consider the atmospheric heat budget with all of the heat fluxes defined in the top of the ocean-ice/snow system. Energy conservation requires

$$Q_{\rm air} = (1-c)Q_{\rm ao} + cQ_{\rm con} \tag{4}$$

where $Q_{\rm ao}$ is the heat flux in the open water portion of the grid point, and c is the ice concentration. Although the value of $Q_{\rm con}$ depends on the effective thickness of the snow-ice layer in the grid box, it is much smaller than $Q_{\rm ao}$. For simplicity, we assume $Q_{\rm con}$ to be 10% of $Q_{\rm ao}$. We will see in the following that the actual value is not important as long as it is small. Eq. (4) can then be simplified as

$$Q_{\rm air} = (1- \ c)Q_{\rm ao} + 0.1cQ_{\rm ao} \equiv (1-0.9c)Q_{\rm ao}. \tag{5}$$

Therefore, we have

$$Q_{\rm ao} = Q_{\rm air}/(1-0.9c). \tag{6}$$

For open ocean where c is zero, we have $Q_{\rm ao} = Q_{\rm air}$. For the ice-presence region, we can estimate the forcing flux $Q_{\rm ao}$ based on (6) from the observed $Q_{\rm air}$ and the observed c and

force the ocean model based on

$$\hat{Q}_{\rm net} = (1-c)Q_{\rm ao} + cQ_{\rm io} \equiv \frac{(1-c)}{(1-0.9\hat{c})}Q_{\rm air} + cQ_{\rm io} \tag{7}$$

where $\hat{c}$ is the observed ice concentration. If the simulated ice concentration c is smaller than the observed $\hat{c}$, the heat flux $\hat{Q}_{\rm net}$ estimated from $Q_{\rm air}$ according to (7) will be larger than $Q_{\rm air}$, until the heat flux extracted from the ocean leads to the ice formation so that the simulated c reaches the observed value. The amount of nudging in this formula is similar to that of the temperature method.

In an additional experiment (Figure 9), we use $\hat{Q}_{\rm net}$ given by (7) to force the ocean model, with $\hat{c}$ set to 0.9 over the climatological ice covered areas shown in Figure 2, and $Q_{\rm air}$ taken to be the da Silva et al.'s climatological heat flux. The agreement of the results in this experiment with those shown in Figure 2 is quite good in all areas, due to the additional nudging from the reformulated forcing. In the GSL there is much more ice and the ice is present in all of the three winters. Although the model still drifts to a higher temperature over the integration in the region, it does form ice in each winter in the three year long integration.

4. Summary and Conclusion

Previous numerical studies of the sea ice on the Labrador and Newfoundland Shelves were made using Hibler's ice model (1979) coupled to ocean circulation models of different complexity (eg. Ikeda et al., 1988; Ikeda et al., 1996; Yao et al., 2000). Those studies demonstrated the ability of coupled ice-ocean models to simulate the seasonal and interannual variations of sea ice in the NWA. The common problem in previous studies is the early and excessive ice melting in the spring.

In this study we use the second version of CICE ice model (Hunke and Lipscomb, 2000) coupled to the regional Northwest Atlantic (NWA) Ocean model of Sheng et al. (2001). The ocean model employs the semi-prognostic method (see Greatbatch et al., 2003) to correct for model drift, allowing us to carry out a multi-year simulation. The CICE ice model uses the elastic-viscous-plastic ice rheology of Hunke and Dukowicz (1997), instead of Hibler's viscous-plastic ice rheology used in previous studies. CICE also

uses Winton's 3-layer thermodynamics, with the brine content of the upper ice represented with a variable heat capacity. The CICE ice model has five ice thickness categories in the standard configuration. In this study, only two ice categories were chosen for simplicity. In addition, different from previous coupled ice-ocean studies, we use different methods to specify the atmospheric heat fluxes over the open water portion of the model grid compared to ice-present regions (see subsection 2.3 for the details). In particular, over open water, we use the net heat flux climatology of de Silva et al.(1994) to drive the ocean model and introduce a parameter γ to represent the degree to which the insulation effect of sea ice is already included in the da Silva et al. climatology. The model works well under this parameterization, although the ice thickness is sensitive to the value of γ, while the area of the ice-covered region is affected in a lesser degree.

Our coupled system simulates reasonably well the annual cycle of sea ice in the NWA, in comparison with the ice coverage climatology constructed by da Silva et al. (1994). In this study, we focus on the roles of the individual physical processes that affect the simulated ice states, instead of getting a best-fit of model results to the observations. Our principal result is that inclusion of the heat capacity of sea ice reduces the early springtime melting of sea ice in the NWA by about 10 days, in better agreement with observations than found in previous studies.

Acknowledgments

We wish to thank Elizabeth Hunke and three anonymous reviewers for their useful suggestions and comments. R.J.G. and J.S. are supported by the Natural Sciences and Engineering Research Council of Canada (NSERC), MARTEC (a Halifax based company), and the Meteorological Service of Canada (MSC) through the NSERC/MARTEC/MSC Industrial Research Chair in "Regional Ocean Modelling and Prediction". Financial support for this work has also been received from the Canadian Foundation for Innovation.

References

Bitz, C. M., M. M. Holland, A. J. Weaver, and M. Eby, Simulating the ice-thickness distribution in a coupled climate model, *J. Geophys. Res., 106*, 2441-2463, 2001.

Bitz, C. M., and W. H. Lipscomb, An energy-conserving thermodynamic model of sea ice, *J. Geophys. Res., 104*, 15669-15677, 1999.

Bryan, K., Accelerating the convergence to equilibrium of ocean-climate model, *J. Phys. Oceanogr., 14*, 666-673, 1984.

Carsey, F. D., S. A. D. Argus, M. J. Collins, B. Holt, C. E. Livingstone, and C. L. Tang, Overview of LIMEX '87 ice observations, *IEEE J. Geosci. Remote Senssing, 27*, 468-482, 1989.

Cox, M. D., A primitive equation 3-dimension model of the ocean, GFDL Ocean Group Tech Rep., 1, GFDL, Princeton, N.J., 350 pp., 1984.

da Silva, A. M., C. C. Young, and S. Levitus, Atlas of surface marine data 1994, Volume 3, Anomalies of heat and momentum fluxes, NOAA Atlas NESDIS 8, NOAA, Washington, DC, 413 pp., 1994.

Davidson, F., R. J. Greatbatch, and B. deYoung, Asymmetry in the response of a stratified coastal embayment to wind forcing, *J. Geophys. Res., 106*, 7001-7016, 2001.

Greatbatch, R. J., A. F. Fanning, A. D. Goulding, and S. Levitus, A diagnosis of interpentadal circulation changes in the North Atlantic, *J. Geophys. Res., 96*, 22009-22023, 1991.

Greatbatch, R. J., J. Sheng, C. Eden, L. Tang, X. Zhai, and J. Zhao, The semi-prognostic method, *Continental Shelf Res.*, in press, 2004.

Haney, R. L., Surface thermal boundary condition for ocean circulation models, *J. Phys. Oceanogr., 1*, 241-249, 1971.

Hibler, W. D., A dynamic thermodynamic sea ice model, *J. Phys. Oceanogr., 9*, 815-846, 1979.

Hibler, W. D., and J. E. Walsh, On modelling seasonal and interannual fluctuation of Arctic sea ice, *J. Phys. Oceanogr., 12*, 1514-1523, 1982.

Holland, D. M., L. A. Mysak, D. K. Manak, and J. M. Oberhuber, 1993: Sensitivity study of a dynamic thermodynamic sea ice model, *J. Geophys. Res., 98*, 2561-2586, 1993.

Hunke, E. C., and J. K. Dukowicz, An elastic-viscous-plastic model for sea ice dynamics, *J. Phys. Oceanogr., 27*, 1849-1867, 1997.

Hunke, E. C., and W. H. Lipscomb, CICE: The Los Alamos Sea Ice Model Documentation and Software User's Manual, T-3 Fluid Dynamics Group, Los Alamos National Laboratory, Tech. Rep. LACC-98-16 v.3, 52 pp., 2000.

Ikeda, M., Numerical modelling of the ocean circulation and ice cover over the continental shelf, *J. Phys. Oceanogr., 21*, 97-117, 1991.

Ikeda, M., G. Symonds, and T. Yao, Simulated fluctuations in annual Labrador sea-ice cover, *Atmos. Ocean, 26*, 16-39, 1988.

Ikeda, M., T. Yao, and Q. Yao, Seasonal evolution of the sea ice cover and shelf water off Labrador simulated in a coupled ice-ocean model, *J. Geophys. Res., 101*, 16465-16470, 1996.

Lipscomb, W. H., Remapping the thickness distribution in sea ice models, *J. Geophys. Res., 106*, 13989-14000, 2001.

Lu, Y., K. R. Thompson, and D. G. Wright, Tidal currents and mixing in the Gulf of St. Lawrence: an application of the incremental approach to data assimilation, *Can. J. Fish. Aquat. Sci., 58*, 723-735, 2001.

Mysak, L. A., S. Peng, and R. G. Wood, Application of a coupled ice-ocean model to the Labrador Sea, *Atmos. Ocean, 29*, 232-255, 1991.

Oberhuber, J. M., Simulation of the Atlantic circulation with a coupled sea ice-mixed layer-isopycnic general-circulation model, *J. Phys. Oceanogr., 23*, 808-829, 1993.

Orlanski, I., A simple boundary condition for unbounded hyperbolic flows, *J. Comput. Phys., 21*, 251-269, 1976.

Peterson, I. K., A snapshot of the Labrador Current inferred from ice-floe movement in NOAA satellite imagery, *Atmos. Ocean, 25*, 402-415, 1987.

Prinsenberg, S. J., I. K. Peterson, and S. Holladay, Comparison of airborne eletromagnetic ice thickness data with NOAA/AVHRR and ERS-1/SAR images, *Atmos. Ocean, 34*, 185-205, 1996.

Saucier, F. J., F. Roy, D. Gilbert, P. Pellerin, and H. Ritchie, Modelling the formation and circulation processes of water masses and sea ice in the Gulf of St. Lawrence, *J. Geophys. Res., 108*, 3269, doi:10.1029/2000JC000686, 2003.

Semtner, A. J., A model for the thermodynamic growth of sea ice in numerical investigations of climate, *J. Phys. Oceanogr., 6*, 379-389, 1976.

Sheng, J., Dynamics of a buoyancy-driven coastal jet: The Gaspé Current, *J. Phys. Oceanogr., 31*, 3146-3163, 2001.

Sheng, J., and L. Tang, A numerical study of circulation in the western Caribbean Sea, *J. Phys. Oceanogr., 33*, 2049-2069, 2003.

Sheng, J., R. J. Greatbatch, and D. G. Wright, Improving the utility of ocean circulation models through adjustment of the momentum balance, *J. Geophys. Res., 106*, 16711-16728, 2001.

Sheng, J., D. G. Wright, R. J. Greatbatch, and D. E. Dietrich, CANDIE: A new version of the DieCAST ocean circulation model. *J. Atmos. Oceanic Technol., 15*, 1414-1432, 1998.

Smolarkiewicz, P. K., A fully multidimensional positive definite advection transport algorithm with small implicit diffusion, *J. Comput. Phys., 54*, 325-362, 1984.

Symonds, G., Seasonal ice extent on the northwest Newfoundland shelf, *J. Geophys. Res., 91*, 10,718-728, 1986.

Tang, C. L., Q. Gui, and B. M. DeTracey, A modeling study of upper ocean winter processes in the Labrador Sea. *J. Geophys. Res., 104*, 23411-23425, 1999.

Thorndike, A. S., D. A. Rothrock, G. A. Maykut, and R. Colony, The thickness distribution of sea ice, *J. Geophys. Res., 80*, 4501-4513, 1975.

Walsh, J. E., W. D. Hibler, and B. Ross, Numerical simulation of North Hemisphere sea ice variability, 1951-1980, *J. Geophys. Res., 90*, 4847-4865, 1985.

Winton, M., A reformulated three-layer sea ice model, *J. Atmos. Oceanic Technol., 17*, 525-531, 2000.

Yao, Q., and S. J. Prinsenberg, Sensitivity tests of 2-category Hibler ice model and comparison to a 10-category Hibler ice model both coupled to a Cox-Bryan ocean model, Can. Tech. Rep. Hydrogr. Ocean Sci., 201, 108 pp., 1999.

Yao, T., and M. Ikeda, A model of Sea Ice and the Upper Ocean Mixed Layer Off Labrador, *J. Geophys. Res., 95*, 11603-11612, 1990.

Yao, T., C. L. Tang, and I. K. Peterson, Modelling the seasonal variation of the sea ice in the Labrador Sea with a coupled multi-category ice model and Princeton Ocean Model, *J. Geophys. Res., 105*, 1153-1165, 2000.

Zhang, S., R. J. Greatbatch, and C. A. Lin, A re-examination of the polar halocline catastrophe and implications for coupled ocean-atmosphere modelling. *J. Phys. Oceanogr., 23*, 287-299, 1993.

Zhang, S., C. A. Lin, and R. J. Greatbatch, A decadal oscillation due to the coupling between an ocean circulation model and a thermodynamic sea-ice model, *J. Mar. Res., 53*, 79-106, 1995.

Received ; revised ; accepted .

List of Figure Captions

Figure 1: Selected topographic features within the coupled ice-ocean model domain of the northwest Atlantic Ocean. Abbreviations are used for Newfoundland (NFLD), Flemish Cap (FC), Scotian Shelf (SS), Gulf of St. Lawrence (GSL), Gulf of Maine (GOM), Hudson Strait (HS), and Strait of Belle Isle (SBI).

Figure 2: Climatological monthly mean ice coverage (dotted areas) from da Silva et al. (1994) in the northwest Atlantic Ocean from December to the next November.

Figure 3: Monthly mean ice thickness (contours) and ice velocity (arrows) from December of the second model year to the next July produced by the coupled ice-ocean modelling system in the control run. Contour intervals are 1.0 m (0.5 m) for the ice thickness greater (less) than 1.0 m, with the 1.0-m thickness highlighted. The ice velocity vectors are plotted at every fourth model grid point.

Figure 4: Monthly mean sea surface temperature (contours) and currents (arrows) from December of the second model year to the next October produced by the coupled ice-ocean modelling system in the control run. Contour intervals are 2°C with 2°C and 10°C highlighted. Extra -1.5°C contours are also added. Velocity vectors are plotted at every fourth model grid point.

Figure 5: (a) Winter mean ice stress (arrows) and net heat flux (contours) at the ice-ocean interface produced by the coupled ice-ocean modelling system in the control run. Contour intervals are 50 Wm^{-2} with both 0 and -200 Wm^{-2} highlighted. (b) Winter mean wind stress (vectors) and net air-ocean heat flux (contours) averaged from monthly mean climatology of da Silva et al. (1994). Contour intervals are 50 Wm^{-2} with 0 and -200 W m^{-2} highlighted. Stress vectors are plotted at every fifth model grid point.

Figure 6: Top panel shows time series of the ice-covered area (thick) and ice volume (thin) produced by the 3-layer (solid) and zero-layer (dashed) thermodynamic ice models. Lower panel shows the difference in ice-covered area (thick) and ice volume (thin) between the zero-layer and 3-layer thermodynamic ice models. The units are 10^9 m^2 and 10^9 m^3 for the ice-covered area and ice volume respectively. The horizontal axis is time in days with 360 model days per year. The shaded area indicates the spring season in Year 3.

Figure 7: Monthly mean ice thickness (contours) and velocity (arrows) produced by the coupled ice-ocean system with $\gamma = 0$ (top), $\gamma = 0.5$ (middle) and $\gamma = 1$ (bottom) (i.e., the ocean gets 100%, 50% and 0% da Silva et al. net heat flux climatology respectively at maximum predicted ice coverage). Contour intervals are 1.0 m (0.5 m) for the ice thickness greater (less) than 1.0 m, with the 1.0-m thickness highlighted. The ice velocity vectors are plotted at every fourth model grid point.

Figure 8: Monthly mean ice thickness (contours) and ice velocity (arrows) produced by the coupled ice-ocean modelling system with (top) the model sea surface temperature restored to the values of 1°C colder than da Silva et al. climatology over the ice-covered area shown in Figure 2 and with (bottom) the coefficient β in Eq. (2) replaced by $(1 - \gamma c)\beta$. The latter case is justified if the restoring term is part of atmosphere forcing fluxes. Contour intervals are 1.0 m (0.5 m) for the ice thickness greater (less) than 1.0 m, with the 1.0-m thickness highlighted. The ice velocity vectors are plotted at every fourth model grid point.

Figure 9: Monthly mean ice thickness (contours) and ice velocity (arrows) produced by the coupled ice-ocean modelling system with the flux formula discussed in subsection 3.6 used to force the coupled model. This formula has an effect of nudging the predicted ice to the observed ice as in the temperature methods. Contour intervals are 1.0 m (0.5 m) for the ice thickness greater (less) than 1.0 m, with the 1.0-m thickness highlighted. The ice velocity vectors are plotted at every fourth model grid point.

Table 1. Selected ice model parameters

Parameters	Values
$1/e^2$ for the elliptical yield curve	0.25
Demarcation thickness between thick/thin ice	0.1 m
Freezing temperature of sea ice	-0.055 × Salinity
Ice stress parameter P	2.75×10^4 Kg m^{-1} s^{-1}
Minimum ice concentration	0.01
Minimum ice thickness	0.01 m
Maximum ice concentration	0.99
Number of ice categories	2
Specific heat of fresh ice	2106 J kg^{-1} K^{-1}
Thermal conductivity of pure ice	2.03 W m^{-1} deg^{-1}
Thermal conductivity of pure snow	0.3 W m^{-1} deg^{-1}
Time scale for ice formation	8 hours
Time scale for ice melting	1 day
Time step for ice dynamics	1 minute
Time step for ice and ocean models	2 hours

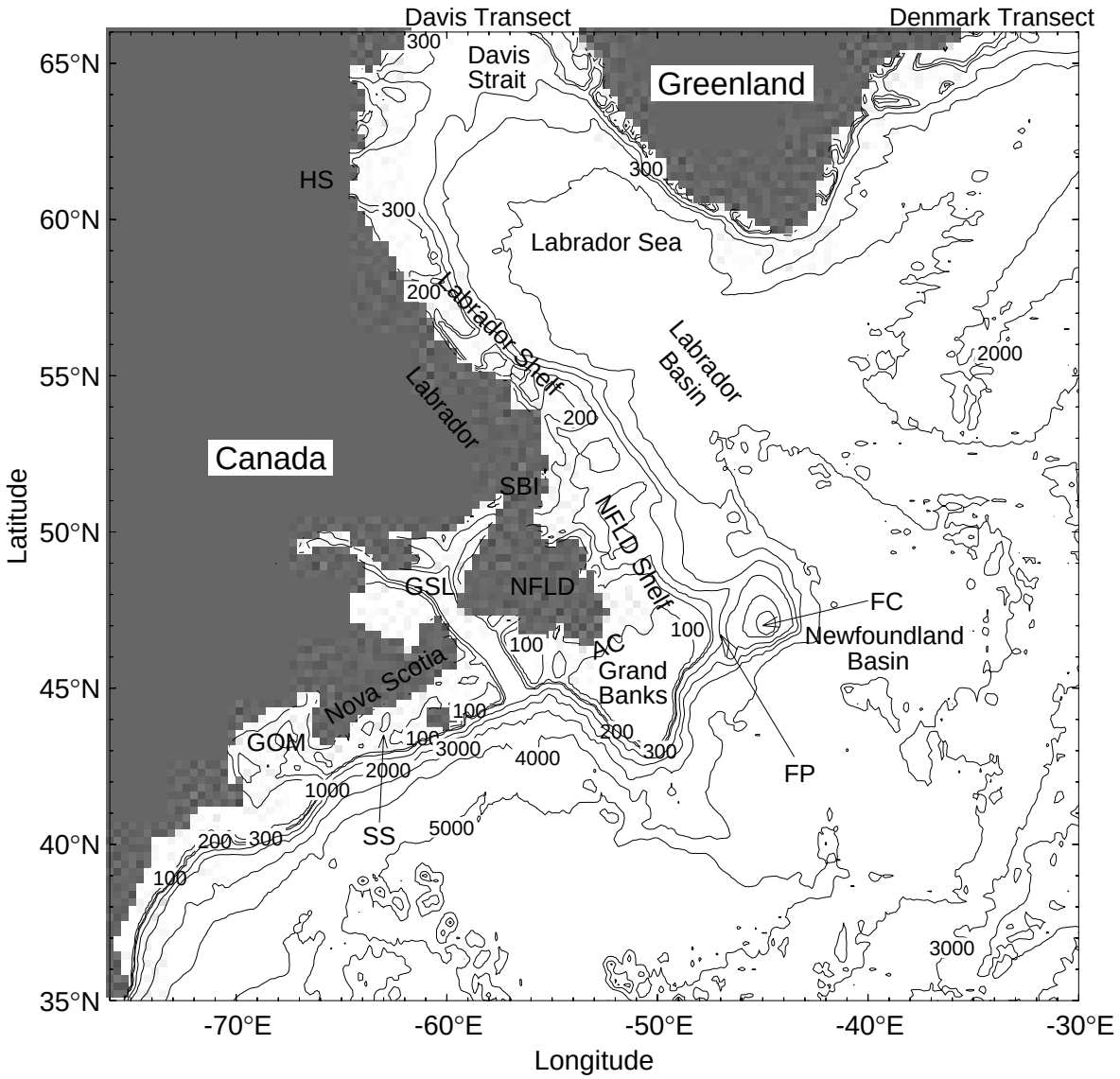

Figure 1. Selected topographic features within the coupled ice-ocean model domain of the northwest Atlantic Ocean. Abbreviations are used for Newfoundland (NFLD), Flemish Cap (FC), Scotian Shelf (SS), Gulf of St. Lawrence (GSL), Gulf of Maine (GOM), Hudson Strait (HS), and Strait of Belle Isle (SBI).

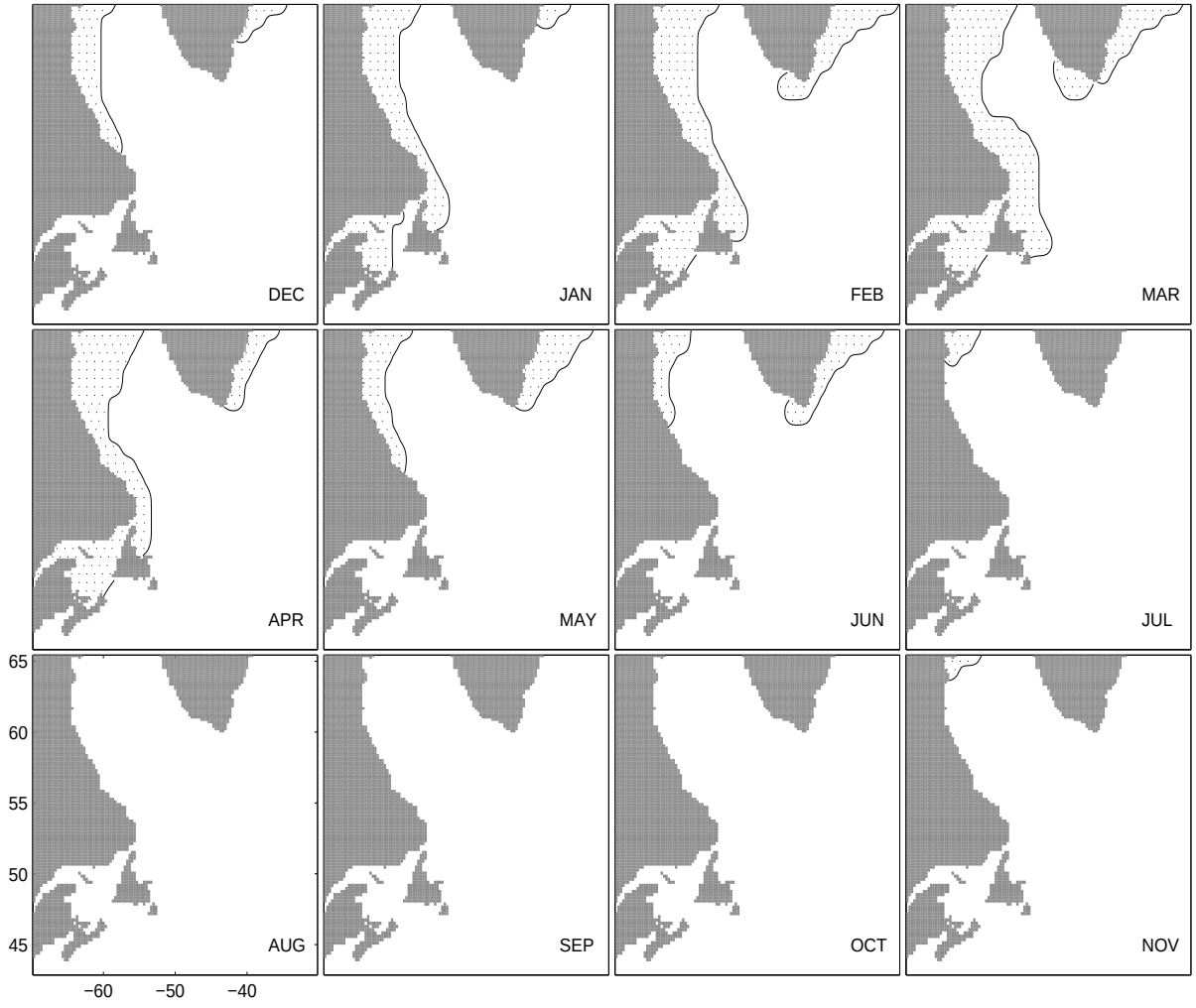

Figure 2. Climatological monthly mean ice coverage (dotted areas) from da Silva et al. (1994) in the northwest Atlantic Ocean from December to the next November.

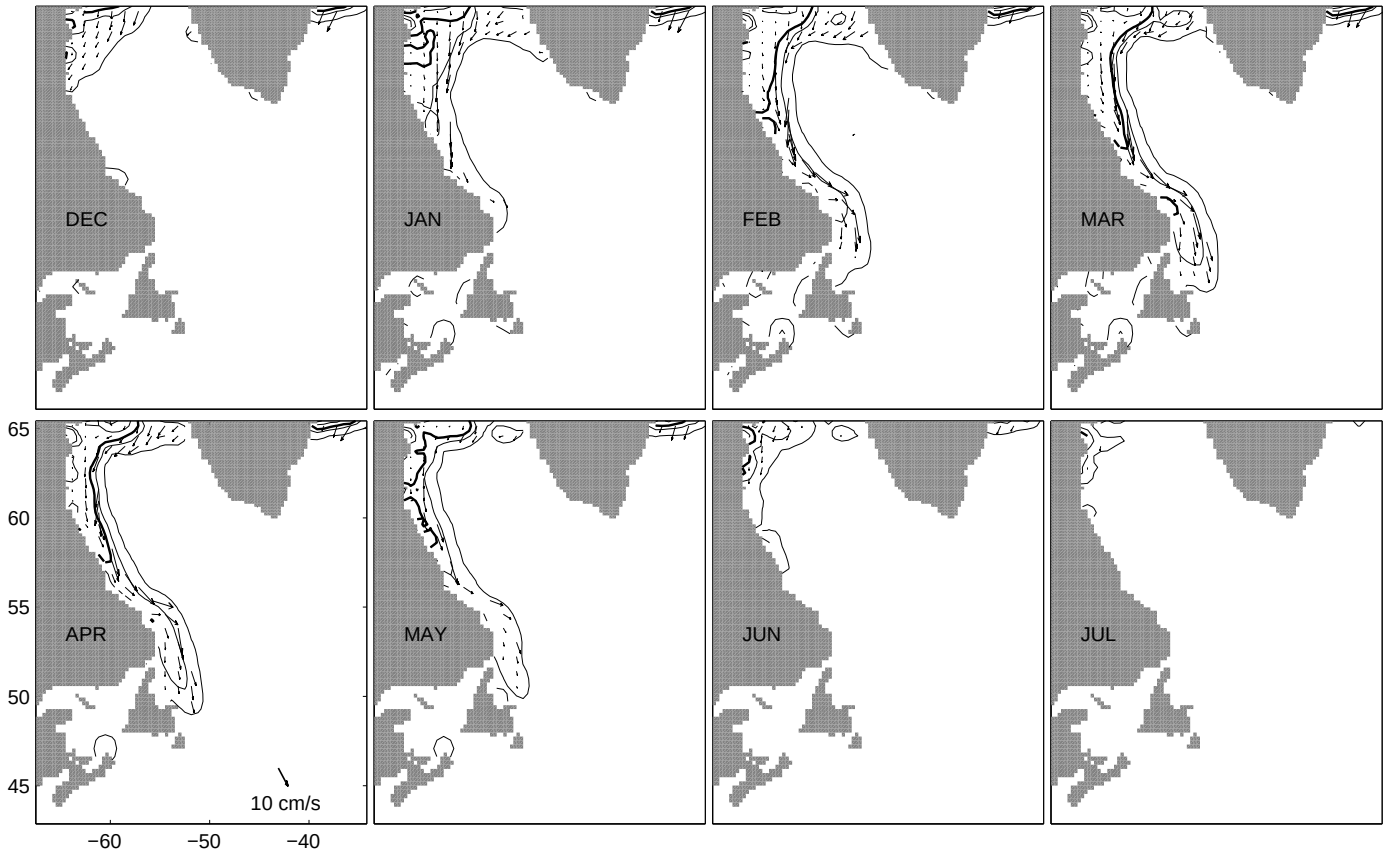

Figure 3. Monthly mean ice thickness (contours) and ice velocity (arrows) from December of the second model year to the next July produced by the coupled ice-ocean modelling system in the control run. Contour intervals are 1.0 m (0.5 m) for the ice thickness greater (less) than 1.0 m, with the 1.0-m thickness highlighted. The ice velocity vectors are plotted at every fourth model grid point.

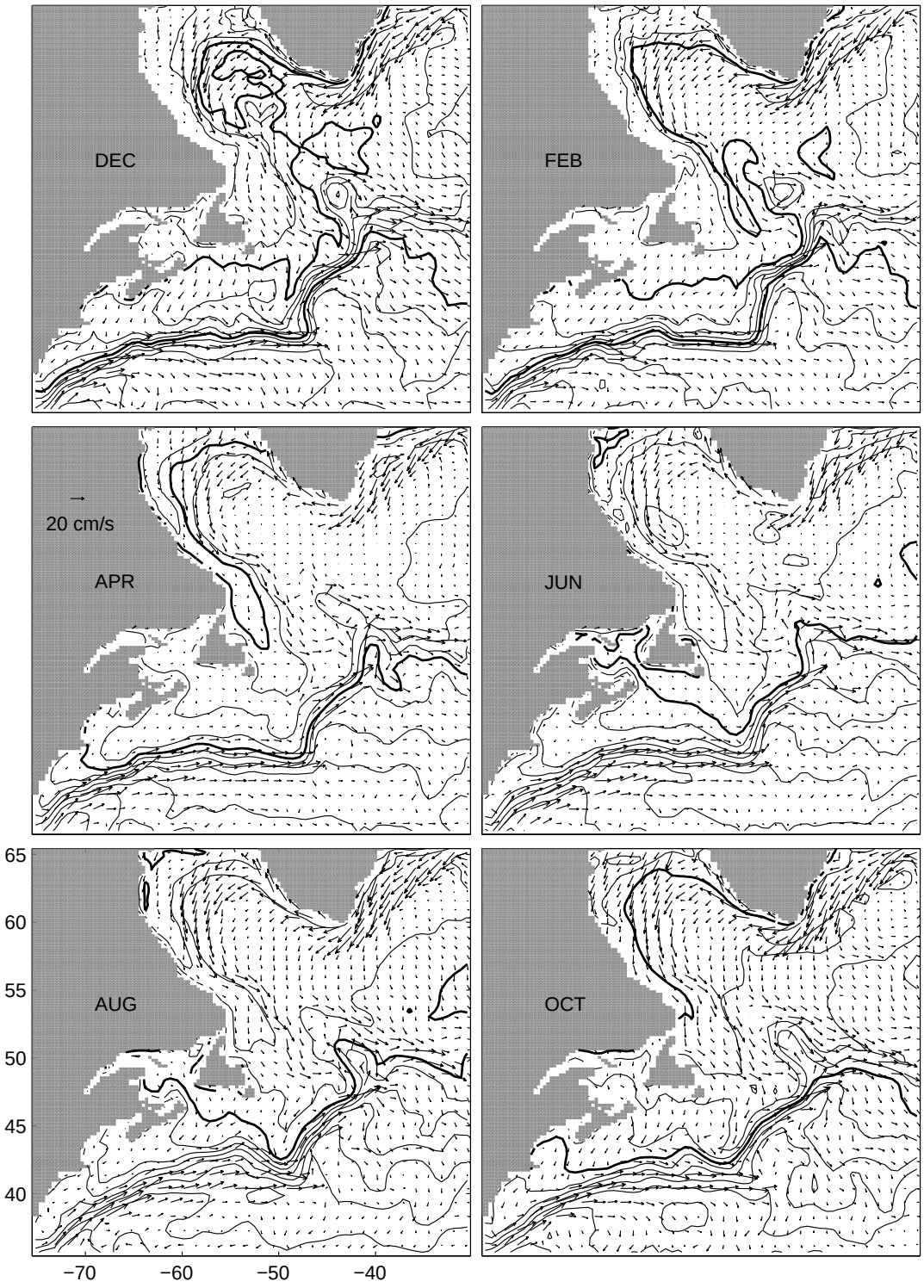

Figure 4. Monthly mean sea surface temperature (contours) and currents (arrows) from December of the second model year to the next October produced by the coupled ice-ocean modelling system in the control run. Contour intervals are 2° C with 2° C and 10° C highlighted. Extra -1.5° C contours are also added. Velocity vectors are plotted at every fourth model grid point.

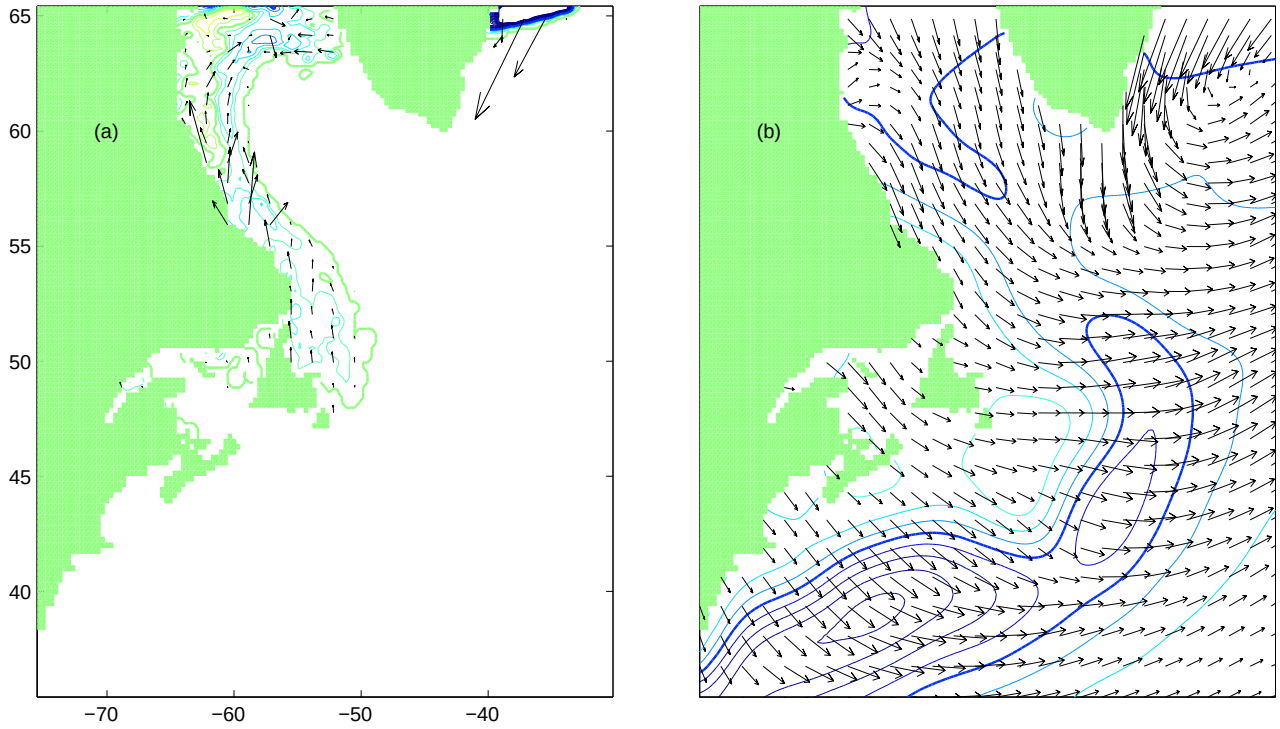

Figure 5. (a) Winter mean ice stress (arrows) and net heat flux (contours) at the ice-ocean interface produced by the coupled ice-ocean modelling system in the control run. Contour intervals are 50 Wm^{-2} with both 0 and -200 Wm^{-2} highlighted. (b) Winter mean wind stress (vectors) and net air-ocean heat flux (contours) averaged from monthly mean climatology of da Silva et al. (1994). Contour intervals are 50 Wm^{-2} with 0 and -200 W m^{-2} highlighted. Stress vectors are plotted at every fifth model grid point.

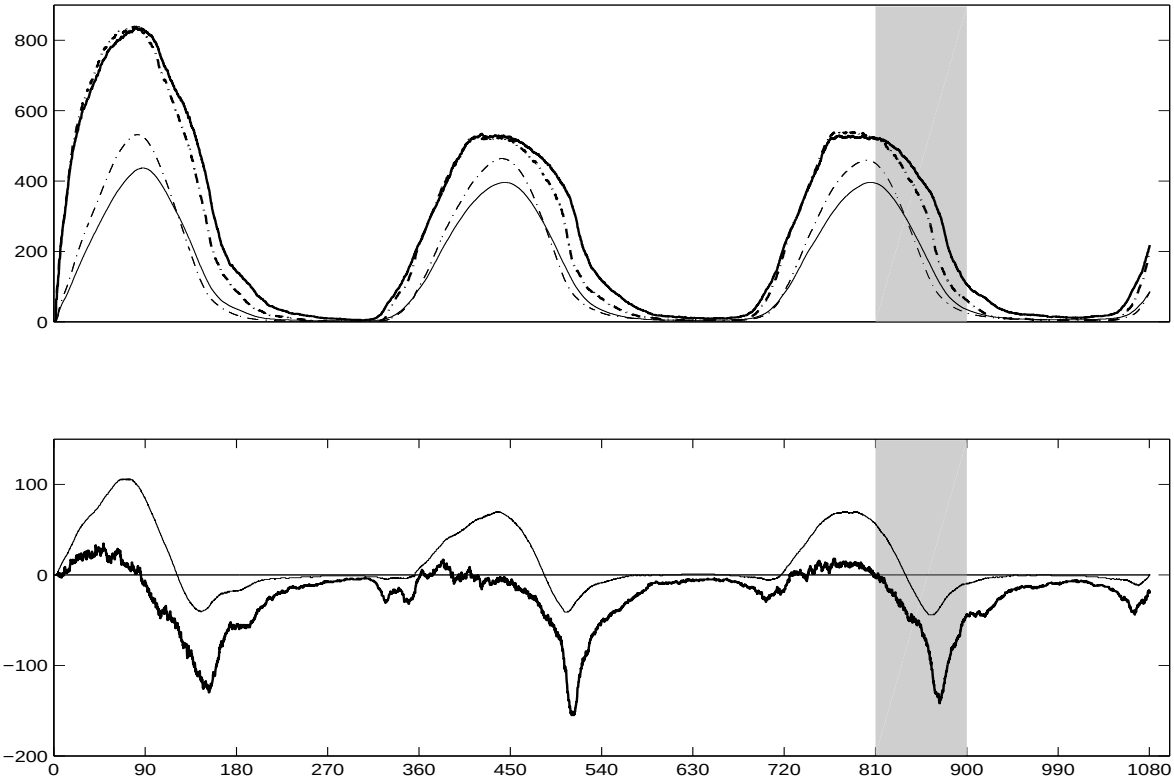

Figure 6. Top panel shows time series of the ice-covered area (thick) and ice volume (thin) produced by the 3-layer (solid) and zero-layer (dashed) thermodynamic ice models. Lower panel shows the difference in ice-covered area (thick) and ice volume (thin) between the zero-layer and 3-layer thermodynamic ice models. The units are 10^9 m^2 and 10^9 m^3 for the ice-covered area and ice volume respectively. The horizontal axis is time in days with 360 model days per year. The shaded area indicates the spring season in Year 3.

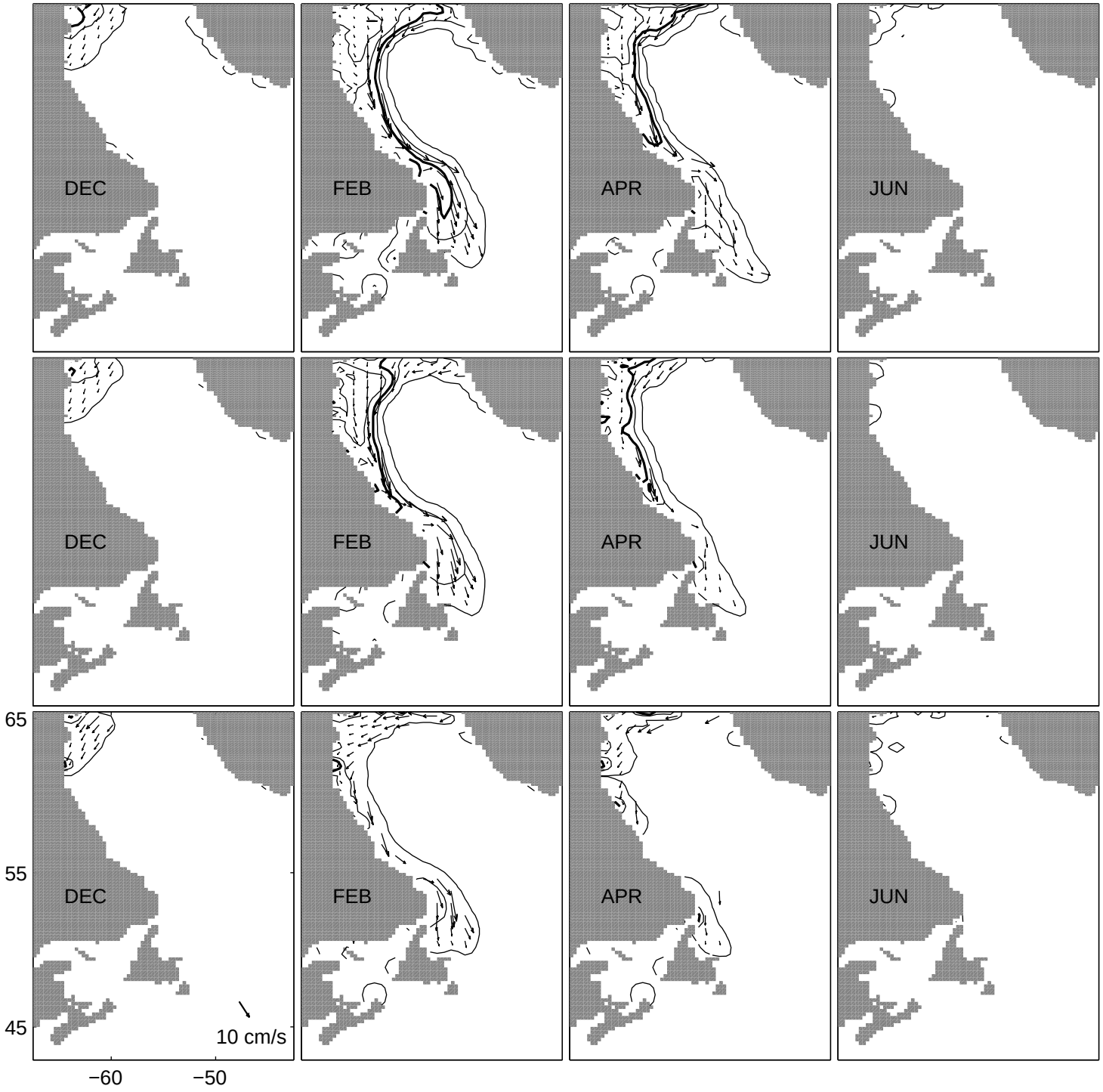

Figure 7. Monthly mean ice thickness (contours) and velocity (arrows) produced by the coupled ice-ocean system with $\gamma = 0$ (top), $\gamma = 0.5$ (middle) and $\gamma = 1$ (bottom) (i.e., the ocean gets 100%, 50% and 0% da Silva et al. net heat flux climatology respectively at maximum predicted ice coverage). Contour intervals are 1.0 m (0.5 m) for the ice thickness greater (less) than 1.0 m, with the 1.0-m thickness highlighted. The ice velocity vectors are plotted at every fourth model grid point.

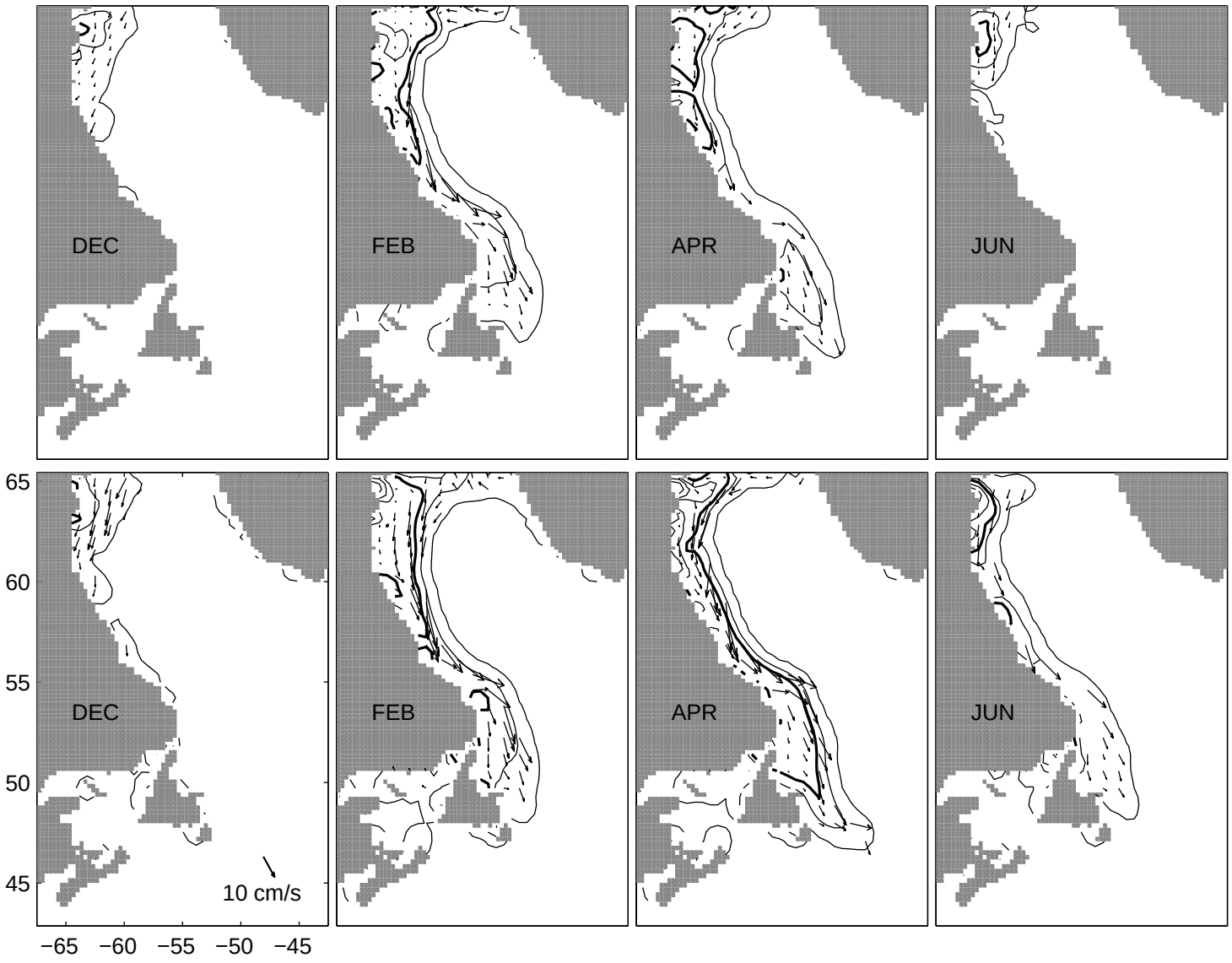

Figure 8. Monthly mean ice thickness (contours) and ice velocity (arrows) produced by the coupled ice-ocean modelling system with (top) the model sea surface temperature restored to the values of 1° C colder than da Silva et al. climatology over the ice-covered area shown in Figure 2 and with (bottom) the coefficient β in Eq. (2) replaced by $(1-\gamma c)\beta$. The latter case is justified if the restoring term is part of atmosphere forcing fluxes. Contour intervals are 1.0 m (0.5 m) for the ice thickness greater (less) than 1.0 m, with the 1.0-m thickness highlighted. The ice velocity vectors are plotted at every fourth model grid point.

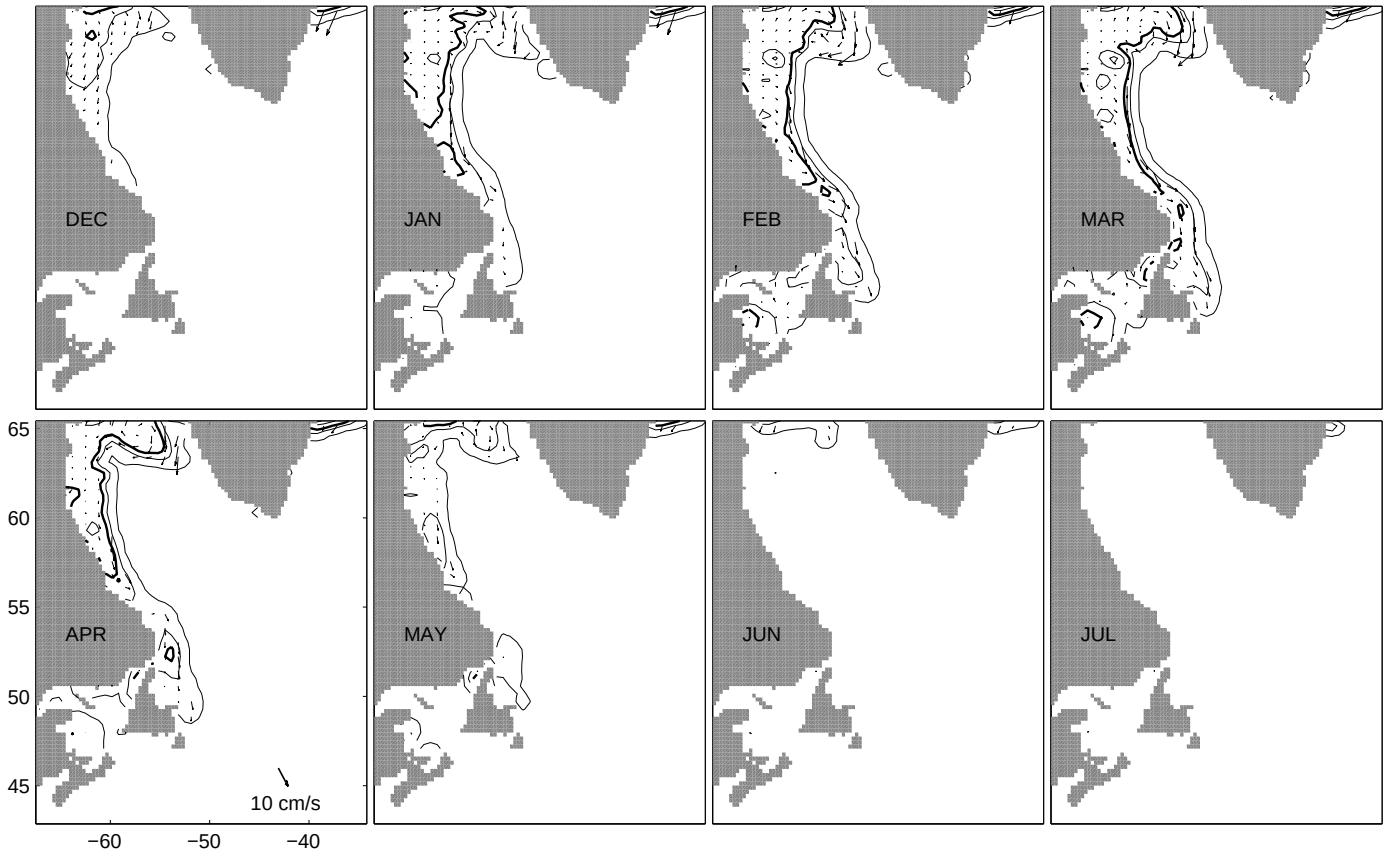

Figure 9. Monthly mean ice thickness (contours) and ice velocity (arrows) produced by the coupled ice-ocean modelling system with the flux formula discussed in subsection 3.6 used to force the coupled model. This formula has an effect of nudging the predicted ice to the observed ice as in the temperature methods. Contour intervals are 1.0 m (0.5 m) for the ice thickness greater (less) than 1.0 m, with the 1.0-m thickness highlighted. The ice velocity vectors are plotted at every fourth model grid point.